

Persistent photoconductance in doping-modulated and compensated *a*-Si:H

Alejandro J. Hamed

The Department of Physics and The James Franck Institute, The University of Chicago, Chicago, Illinois 60637

(Received 29 November 1990)

We present experimental results and numerical calculations in support of the following model to explain the origin of the persistent-photoconductivity effect (PPC) in *p-n* multilayers of hydrogenated amorphous silicon (*a*-Si:H): Small light exposures create Staebler-Wronski defects in the *p*-type regions of the multilayer, making these regions more intrinsic. This brings the equilibrium Fermi level of the multilayer closer to the conduction band in the depletion zones of the *n*-type regions, causing an increase in the conductance of the layered structure when the conductance is electron dominated. At large light exposures, the Staebler-Wronski defects created in the *n*-type regions pull the Fermi level away from the conduction band, decreasing the conductance of the film. Our experimental results show that, for a given light intensity, the creation rate and annealing kinetics of the PPC in multilayers are correlated with the creation rate and annealing kinetics of the light-induced conductance changes in unlayered *p*-type and *n*-type *a*-Si:H films having the same dopings as the *p*-type and *n*-type regions in the multilayer. The PPC follows a stretched-exponential time relaxation with the same parameters describing the decays of other metastable conditions in *a*-Si:H. Our computer calculations can reproduce the dark conductivity and magnitude of the PPC in a multilayer (doped at 100 ppm) as a function of sublayer thickness *d*, except for *d* < 20 nm. The calculated values can be made to agree with the measured ones at *d* < 20 nm by letting the defect structure of the doped *a*-Si:H in the multilayer change with decreasing *d* for *d* < 20 nm. Photothermal-deflection-spectroscopy measurements show that indeed the concentration of defects in the multilayer decreases with decreasing *d* for *d* < 20 nm. We find that the rate of creation and annealing kinetics of the PPC in multilayers with *d* < 20 nm is correlated with the rate of creation and annealing kinetics of the light-induced conductance changes in unlayered *a*-Si:H films having smaller gas-phase doping levels than the ones used in depositing the multilayers. Compensated films appear to behave similarly to multilayers with small *d*. The model proposed for PPC in multilayers can explain all the experimental facts associated with the effect and is extended to account for the light-induced conductance changes in compensated and other layered films, like *n-i-n-i*, *p-i-p-i*, and *n-i-p-i* multilayers.

I. INTRODUCTION

Considerable effort has been dedicated to understanding the origin of the persistent-photoconductivity effect (PPC) in doping-modulated and compensated films of hydrogenated amorphous silicon (*a*-Si:H).¹⁻²⁴ The doping-modulated films, or *p-n* multilayers, consist of alternating *n*-type and *p*-type doped layers of *a*-Si:H, while the compensated samples are prepared by simultaneously doping an *a*-Si:H film with donor and acceptor species. The PPC effect, first observed in *a*-Si:H compensated films by Mell and Beyer¹ and in *a*-Si:H multilayers by Kakalios and Fritzsche,² consists of a metastable increase in dark conductivity caused by a brief light exposure. The excess conductance can exceed the conductance of the equilibrium state by up to three orders of magnitude and decays on the time scale of weeks at room temperature.

The magnitude of this PPC is only surpassed by that observed in *a*-Si:H/*a*-SiN_x:H multilayers. Recently, Hamed and Fritzsche²⁵ reported excess conductances that are 10⁵ times larger than the conductance of the annealed state for these compositionally modulated films at room temperature, and explained the effect in terms of metastable changes in the silicon nitride defect structure.

A PPC had previously been predicted and observed in crystalline doping-modulated superlattices.²⁶ This effect, which can be created only at low temperatures and is of smaller magnitude, the excess conductivity being only a fraction (≈ 0.5) of the equilibrium conductivity value, was successfully explained in terms of the internal potential barriers that inhibit the recombination of the photoexcited electrons and holes spatially separated during illumination by the associated internal electric fields. This field-separation mechanism, however, fails to explain several experimental facts about the PPC observed in *a*-Si:H doping-modulated multilayers. The magnitude and long decay times observed at room temperature in this case,² the low quantum efficiency,² and the activated behavior^{3,7} for the production of the PPC cannot be understood in terms of the field-separation model. In fact, it was shown later that the internal barriers in the multilayer could keep the field-separated photocarriers from recombining only at temperatures below a few tens of degrees, and that the PPC observed above, say, 80 K has a different origin.⁷

The various models originally proposed to explain the PPC effect in *a*-Si:H doping-modulated and compensated films^{1,2,6-8,10,12,17,18} invoked the existence of some sort of

trapping center that would capture photoexcited holes and not release them on account of an energy barrier or lattice relaxation process, leaving the n -type regions of the composite a -Si:H films with an excess concentration of electrons responsible for the PPC.

More recently, in a different approach, Kakalios and Street^{13,22} explained the effect in these composite materials in terms of the thermal equilibration model for a -Si:H. They proposed that the p - n junction fields spatially separate photoexcited holes and electrons to the p - and n -type regions, respectively, giving rise to an excess density of occupied band-tail states. According to these authors, some fraction of the spatially separated holes in the p -type regions will interact with the defect structure during illumination at a faster rate than the electrons will do in the n -type regions. The excess holes that are lost due to the equilibration of the defect structure in the p zones are immobile and thus unable to recombine with the spatially separated electrons at the p - n -junction interfaces. Thus, once the illumination is stopped, there will be a net excess density of electrons in the n -type layers that accounts for the PPC. As possible mechanisms by which the excess holes interact with the defect states, they mentioned



or



where h denotes a hole occupying a valence-band-tail state, B_4^- and Si_4^0 are fourfold-coordinated negatively charged boron and neutral silicon atoms, respectively, B_3^0 is a threefold-coordinated neutral boron atom, and D^+ is a positively charged Si dangling bond. Reaction (1) was considered to be more likely.²² This model has the advantage of explaining the PPC in terms of changes in the defect structure and/or active dopant concentration without having to postulate the existence of a novel trapping center.

This feature is shared by a model later proposed by Hamed and Fritzsche,^{21,23} which explains the PPC effect in terms of the Staebler-Wronski defects²⁷ created by light in the p -type regions of the material and the consequent change in the position of the Fermi level in the composite. We have already presented some preliminary data in support of this model.^{21,23} In this work we present more complete experimental results as well as numerical calculations that appear to support our model.

We begin in Sec. II by stating the model, its assumptions and predictions. After a brief description of experimental details in Sec. III, we compare in Sec. IV A the creation rate and annealing kinetics of the PPC effect in multilayers with the creation rate and annealing kinetics of the conductance changes due to Staebler-Wronski defects in unlayered p -type and n -type films having the same doping as the p -type and n -type regions in the multilayers. In Sec. IV B we study the time relaxation of the PPC effect and compare it with the decay of metastable changes produced by a variety of means in the gap-state distribution of unlayered a -Si:H.

In Sec. IV C we carry out numerical calculations based on our model. In particular, we obtain the conductivity of a multilayer as a function of sublayer thickness d and the magnitude of the PPC effect as a function of d for a given Gaussian distribution of Staebler-Wronski defects in the p -type regions. The agreement between calculated and experimental values turns out to be very good, except for multilayers with very small values of d ($d < 20$ nm). Agreement between calculations and experiments can be achieved at small d by letting the gap-state distribution and/or doping efficiency change with d in the range $d < 20$ nm. In order to test this idea, we report in Sec. IV D measurements of the density of dangling bonds in a multilayer as a function of d by means of photothermal deflection spectroscopy (PDS).

In Sec. IV E we focus on multilayers having $d < 20$ nm, and we measure the creation rate and annealing kinetics of the PPC in two of these multilayers, and compare them in Sec. IV F with the creation rate and annealing kinetics of the light-induced conductance changes in a series of unlayered p -type and n -type films of decreasing doping level. In Sec. IV G we present results for compensated films and compare them with those in multilayers having small sublayer thickness. We conclude the presentation of experimental results in Sec. IV H, where we make a brief digression to discuss some high-bias anomalies in the conductivity of the multilayers that may lead to a misjudgement of the magnitude of the PPC in these samples if one is not aware of these effects.

The discussion of the results is carried out in Sec. V, where we present a more general version of the model to include the PPC effect in compensated films and in multilayers with very small sublayer thickness (with respect to the depletion lengths) as well as the light-induced conductance changes in other a -Si:H multilayers containing intrinsic (i) layers, like n - i - n - i , p - i - p - i , and p - i - n - i - p - i - n . A short summary concludes the paper.

II. THE MODEL

We review here the main ideas and predictions of a simple model we proposed earlier^{21,23} to explain the PPC effect observed in doping-modulated a -Si:H multilayers. The model is as follows. At small light exposures, light creates Staebler-Wronski defects in the p -type regions of the multilayer, making these regions more intrinsic, while no significant change takes place yet in the defect structure of the n -type layers. As a consequence of this, the new equilibrium Fermi level of the layered structure is brought closer to the conduction band in the depletion zones of the n -type layers, causing an increase in the conductance when it is electron dominated. At large light exposures, on the other hand, the number of Staebler-Wronski defects created in the n -type material becomes large enough to pull the Fermi level away from the conduction band in the n regions, thus decreasing the magnitude of the PPC and at very large exposures, producing even a net conductance decrease.

This model does not require any special hole traps and explains the PPC effect in terms of the excess concentrations of dangling bonds created *directly* by light that also

occur and can be verified in unlayered p -type and n -type films. By *directly* we mean that it is the excess carriers photogenerated by light in the p -type regions of the multilayer that determine to what extent the defect structure of these regions is altered. In this picture, the field-separated photocarriers represent a negligible fraction of the excess carrier concentrations for the light intensities typically used to produce the effect.

Thus, if we compare the creation rates of the PPC in a multilayer and of the light-induced conductance decrease in unlayered p -type and n -type films having the same doping levels as the regions in the multilayer, we should see the following. For a fixed light intensity, the conductivity of the multilayer should increase with exposure time, while the conductivity of the unlayered p -type film decreases. At long exposure times, when the conductance of the unlayered n -type film begins to decrease, the conductivity of the multilayer should decrease as well.

The model implies that the temperatures at which the PPC effect in the multilayer and the Staebler-Wronski defects in the p -type film are eliminated by annealing should be the same, and the annealing temperature of the Staebler-Wronski defects in the n -type film should coincide with the annealing point of the conductivity decrease observed in the multilayer after large exposures. We also expect the time relaxation of the PPC to be similar to the decay of the light-induced excess concentration of dangling bonds observed in unlayered a -Si:H films. Finally, we expect the ratio of the conductivity in the PPC state to the conductivity of the annealed state (before illumination) to be of order unity when the sublayer thickness of the multilayer is made much larger than the depletion lengths in the n -type regions and conduction becomes dominated by the bulk or nondepleted n -type zones. It is not as clear, however, what the value of this ratio will be at very small sublayer thicknesses, and the answer will come from the computer calculations in Sec. IV C. In the next sections we present experimental results in support of the ideas and consequences of this model.

III. EXPERIMENTAL DETAILS

The samples for this study were deposited, using a single glow-discharge chamber, on 7059 Corning glass substrates held at 220 °C. We prepared a series of five doping-modulated a -Si:H films, denoted $m1$ – $m5$, of varying sublayer thickness d as described in Table I. The p - and n -type layers of the multilayer were made using

100 ppm of diborane and phosphine, respectively, in silane. In the case of sample $m5$, each p - and n -type layer is 8 nm thick, followed by 2 nm of completely compensated material obtained by simultaneously admitting in the chamber a 1:1 mixture of the gases used for the p - and n -type layers. Special care was taken to avoid cross contamination when making the multilayers: after completion of a layer, a protective shutter was used to cover the samples, and the admission of a new gas mixture was followed by 1–3 min of closed-shutter deposition before opening the shutter to proceed with the next layer. Four p -type, five n -type, and two compensated unlayered films, samples $c1$ and $c2$, were also prepared, and the corresponding doping levels are listed in Table II. We denote the p -type and n -type films as follows: $p1$ is the p -type film doped at 1 ppm, $p10$ is the p -type film doped at 10 ppm, $n0.1$ is the n -type film doped at 0.1 ppm, and so on. The numbers used to denote the multilayers and compensated films have no particular meaning. All unlayered films are about 1 μm thick.

Contacts having a length of 0.5 cm and a gap of 0.2 cm were evaporated on top of the sample for coplanar conductance measurements. The multilayers were previously scratched with a diamond scribe to insure electrical contact to all layers. Ni-Cr contacts were used for the p -type and compensated samples, while Mg was used with the multilayers and the n -type films to obtain Ohmic current-voltage characteristics. The soft Mg electrodes were covered with an overlayer of Ni-Cr to protect them from fast oxidation and mechanical damage. The p -type films were etched in a solution of hydrofluoric acid, 25% volume in water, for 20 s to eliminate oxide layers that generate highly conductive hole accumulation surface regions.²⁸ The samples were annealed at temperatures between 170 and 190 °C for 20 min in vacuum to eliminate adsorbates²⁹ and previous light effects. To illuminate the samples we used white light from a tungsten-halogen lamp having an intensity of 80 mW cm^{-2} in the spectral range 600 nm $< \lambda < 800$ nm. In the annealing studies, the heating and cooling rates were about 0.05 °C s⁻¹. The conductivity of the multilayers was calculated using the total thickness of the film.

IV. RESULTS

For the purpose of characterizing our samples, Tables I and II provide the room-temperature conductivity σ_a and photoconductivity σ_p as well as the high-

TABLE I. Description and electronic properties of the multilayers. The asterisk denotes that the last 2 nm of each layer in this multilayer were made of compensated material (see text).

Sample	Periods	d (nm)	σ_a ($\Omega^{-1}\text{cm}^{-1}$)	E_a (eV)	σ_p ($\Omega^{-1}\text{cm}^{-1}$)
$m1$	4	100	6.0×10^{-4}	0.31	5.3×10^{-3}
$m2$	7	36	1.6×10^{-7}	0.65	1.5×10^{-2}
$m3$	30	10	5.9×10^{-10}	0.62	2.1×10^{-4}
$m4$	20	2	1.7×10^{-12}	0.81	3.3×10^{-6}
$m5$	10	10*	9.0×10^{-10}	0.62	1.5×10^{-4}

TABLE II. Electronic properties of unlayered samples.

Sample	Doping	σ_a ($\Omega^{-1}\text{cm}^{-1}$)	E_a (eV)	σ_p ($\Omega^{-1}\text{cm}^{-1}$)
<i>p</i> 1	1.0 ppm B_2H_6	6.4×10^{-11}	0.78	1.3×10^{-5}
<i>p</i> 10	10 ppm B_2H_6	2.5×10^{-10}	0.75	1.7×10^{-5}
<i>p</i> 100	100 ppm B_2H_6	1.4×10^{-8}	0.71	3.7×10^{-5}
<i>p</i> 53	53 ppm B_2H_6	4.5×10^{-9}	0.71	3.0×10^{-5}
<i>n</i> 0.1	0.1 ppm PH_3	1.7×10^{-8}	0.72	2.4×10^{-4}
<i>n</i> 1	1.0 ppm PH_3	1.0×10^{-7}	0.63	3.5×10^{-4}
<i>n</i> 10	10 ppm PH_3	6.7×10^{-4}	0.38	
<i>n</i> 100	100 ppm PH_3	5.9×10^{-3}	0.23	9.2×10^{-3}
<i>n</i> 530	530 ppm PH_3	1.3×10^{-2}	0.37	1.3×10^{-2}
<i>c</i> 1	100 ppm B_2H_6 , 100 ppm PH_3	7.7×10^{-12}	0.85	
<i>c</i> 2	53 ppm B_2H_6 , 530 ppm PH_3	6.5×10^{-6}	0.64	6.0×10^{-4}

temperature activation energy E_a for each of them. Thermopower measurements indicate that all multilayers listed in Table I are *n*-type, that is, the majority carriers are electrons in the *n* layers. As mentioned before, all multilayers have *n*-type and *p*-type regions doped at 100 ppm, and only the sublayer thickness d is varied.

Figure 1 shows the PPC effect for multilayer *m*2. What is shown is the conductance before, during, and after exposing the sample to 30 s of illumination. After turning the light off, there is a fast decay of the photoconductivity followed by a slowly relaxing excess conductivity that is some three orders of magnitude larger than the conductivity before illumination. The relaxation process takes several weeks at room temperature.

A. Creation rate and annealing kinetics

In this section we look at the creation rates and annealing kinetics of the light-induced conductance changes in

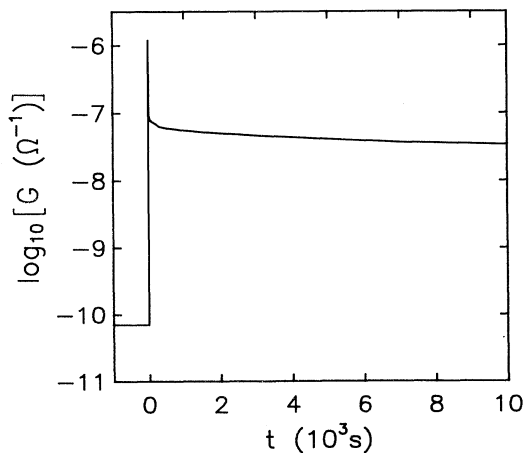


FIG. 1. PPC effect in multilayer *m*2. The conductance before, during and after a 30-s exposure to 80-mW/cm² white light ($600\text{ nm} < \lambda < 800\text{ nm}$) is shown.

multilayers and unlayered *p*-type and *n*-type films. Figure 2 compares the conductivity changes of films *p*100 and *n*100 with those in multilayers *m*1 and *m*2, having $d=100$ and 36 nm, respectively, as a function of exposure time t_e to our light source at room temperature. The conductivity σ is measured in each case 5 min after exposure, when the initial fast decay of the photoconductivity has ended and the dark conductivity is slowly relaxing to the conductivity σ_a of the annealed state. The arrows in Fig. 2 point to the values of σ_a .

As shown in Fig. 2, the changes in conductivity with t_e are quite similar for multilayers *m*1 and *m*2. There is a continued increase in σ for $t_e < 10^2$ s, then a small decrease for $10^2\text{ s} < t_e < 10^3$ s followed by a big drop for $t_e > 10^3$ s. Even though the relative changes σ/σ_a in conductivity are much larger for *m*2, the absolute

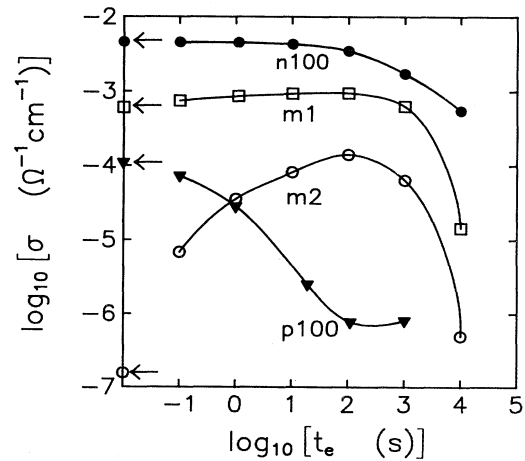


FIG. 2. Dark conductivity σ as a function of exposure time t_e at room temperature for multilayers *m*1 and *m*2, and unlayered films *n*100 and *p*100. Values are obtained 5 min after exposure. Arrows indicate the conductivities σ_a of the annealed state.

changes $\sigma - \sigma_a$ are very similar for both samples. For example, for $t_e = 10^2$ s, the value of σ / σ_a is about 10^3 for $m2$ and only 1.5 for $m1$. However, $\sigma - \sigma_a$ is of the order of 10^{-4} cm^{-1} for both samples.

We observe in Fig. 2 that as $p100$ becomes more resistive with increasing t_e for $t_e < 10^2$ s, the multilayers become more conductive, while little change is observed in the conductivity of $n100$. At $t_e = 10^2$ s the conductance decrease saturates in $p100$, and so does the conductance increase in the multilayers. For $t_e > 10^2$ s the conductivity of $n100$ decreases by a significant amount, and so does the conductivity of the multilayer. Curves similar to those in Fig. 2 were also obtained at $T = 70^\circ\text{C}$. At this temperature, however, the exposure time required to saturate the conductance decrease in $p100$ and the conductance increase in the multilayers is only $t_e = 10$ s. Figure 2 suggests that the observed σ in the multilayers is the superposition of two opposite effects, one that tends to increase and one that tends to decrease the conductivity with increasing light exposure. The first one coincides with changes in the p -type film and the second with changes in the n -type film.

Now we consider the annealing behavior of the conductance changes. Figure 3 compares the annealing curve of the PPC state in multilayer $m2$ (solid line in Fig. 3) with the annealing curves of the Staebler-Wronski defects in films $p100$ and $n100$ after $t_e = 10^3$ s. Again, the annealing behavior of multilayer $m2$ indicates the presence of two simultaneous effects: a metastable excess conductance that anneals at $T_1 = 105^\circ\text{C}$ and a metastable conductance decrease that anneals at the higher temperature $T_2 = 160^\circ\text{C}$. The temperature $T_1 = 105^\circ\text{C}$ coincides with the temperature $T_p = 105^\circ\text{C}$ at which the Staebler-Wronski defects in film $p100$ are eliminated by annealing, and $T_2 = 160^\circ\text{C}$ is very close to the annealing point $T_n = 150^\circ\text{C}$ of the Staebler-Wronski defects in film $n100$.

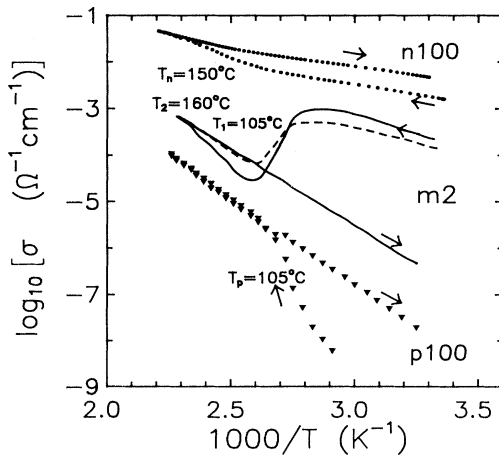


FIG. 3. Annealing curves of the PPC states in multilayer $m1$ obtained after $t_e = 10^3$ s (solid line) and $t_e = 10$ s (dashed line). Also shown are the annealing curves of the Staebler-Wronski defects in unlayered films $p100$ and $n100$ after $t_e = 10^3$ s.

We also notice that the excess conductance obtained in multilayer $m2$ after an exposure time $t_e = 10$ s, which is not enough to alter the conductivity of film $n100$, anneals again at $T_1 = 105^\circ\text{C}$ (dashed line in Fig. 3), but there is no metastable conductance decrease above this temperature. Multilayer $m1$ behaves in the same manner as $m2$. All the annealing temperatures referred to above depend on the heating rate. As pointed out earlier, the heating and cooling rates used in the present study were $0.05^\circ\text{C s}^{-1}$. The results of this section are clearly in agreement with the ideas of the model presented in Sec. II.

B. Time relaxation of the PPC

Metastable changes in the defect structure of $a\text{-Si:H}$ can be produced by a number of means, including light,^{27,30-33} current,³⁴⁻³⁶ rapid cooling from high temperatures,³⁷⁻⁴⁰ and application or existence of high electric fields.⁴¹⁻⁵⁰ The time relaxation of several of these metastable conditions has been measured in the past.^{38,44,51} In all cases it was found that the decay follows a stretched exponential:

$$\delta(t) = \delta_0 \exp \left[- \left(\frac{t}{\tau} \right)^\beta \right], \quad (3)$$

with β showing a linear dependence on temperature and τ being thermally activated. Here δ denotes a generic quantity that measures or reflects the changes in the defect structure.

Thus, in the decay of light-induced defects in undoped $a\text{-Si:H}$ one observes⁵¹ $\beta = T/T_0$ with $T_0 = 600$ K, and $\tau = \tau_0 \exp(E_a/kT)$ with $\tau_0 = 1.8 \times 10^{-10}$ s and $E_a = 0.94$ eV. For the decay of high bias induced changes in the defect structure, the values of these parameters are⁴⁴ $T_0 = 600$ K, $E_a = 1.27$ eV, and $\tau_0 = 2.3 \times 10^{-13}$ s. Similar results are observed in the decay of excess band-tail carriers in doped (1 at. % P) $a\text{-Si:H}$ due to thermal quenching.³⁸

The observed behavior has been accounted for in the hydrogen glass model for $a\text{-Si:H}$,^{44,52} which predicts $T_0 \approx 650$ K and $E_a \approx 1$ eV. According to this model, the decay kinetics of the metastable changes in the defect structure of $a\text{-Si:H}$ is related to the dispersive diffusion of hydrogen in the material, and the motion of hydrogen is the mechanism responsible for the process of creation and annealing of defects. It is then of interest to find out if the relaxation of the PPC effect is similar to the decay of the metastable changes in the defect structure of $a\text{-Si:H}$.

The symbols in Fig. 4(a) show the time decay of the light-induced excess conductance in multilayer $m2$ at the temperatures [from left to right in Fig. 4(a)] 90, 80, 70, 60, and 40°C . The exposure time was 100 s in each case. The solid curves are the result of least-squares fits of stretched exponentials to the data points. Note that the decays are followed over several orders of magnitude in conductance and time. The fits are very satisfactory except at small times for $T = 40^\circ\text{C}$ and at large times for $T = 90^\circ\text{C}$. Figure 4(b) shows the temperature dependence of the β parameter. The line shown is a least-

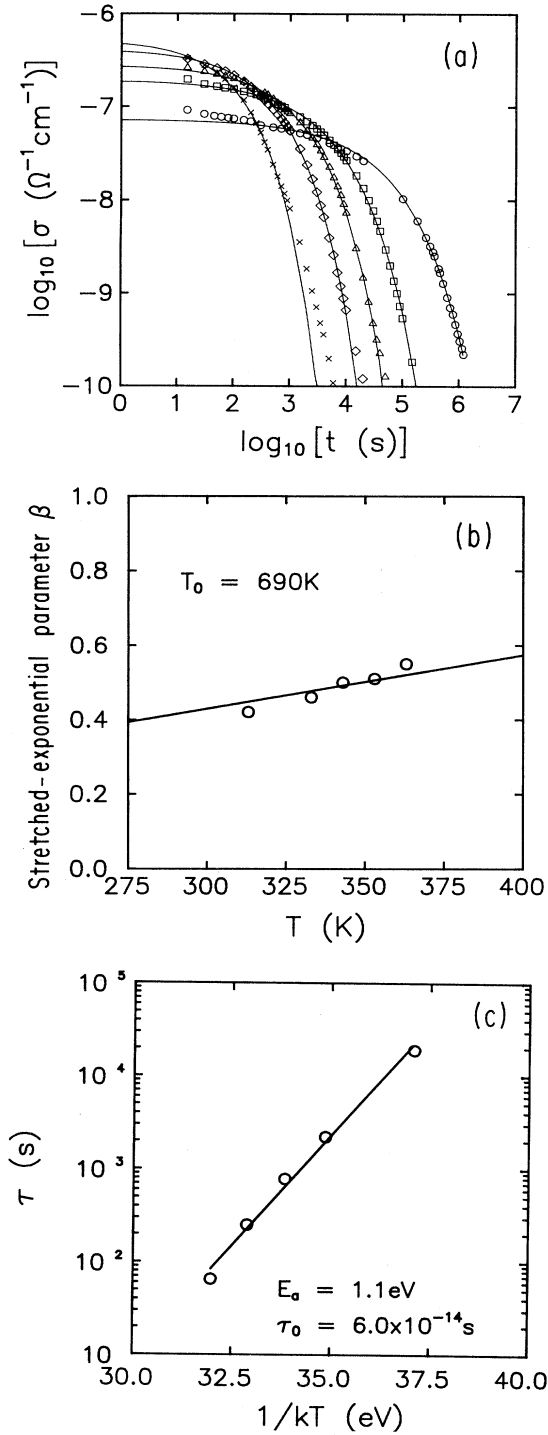


FIG. 4. (a) Decay of the excess conductivity of the PPC state in sample *m2* at the temperatures (from left to right) 90, 80, 70, 60, and 40°C. Symbols are experimental points. The lines are stretched-exponential fits to the data. (b) Temperature dependence of the β parameter obtained from the fits in (a). The line is a least-squares fit to the data points and the origin. T_0 is the inverse slope. (c) Temperature dependence of the τ parameter obtained from the fits in (a). The line, a least-squares fit to the data points, has the activation energy E_a and prefactor τ_0 indicated.

squares fit to the data points including the origin. It yields an inverse slope $T_0=690 \text{ K}$. Figure 4(c) reveals that τ is indeed thermally activated with $E_a=1.1 \text{ eV}$ and $\tau_0=6.0 \times 10^{-14} \text{ s}$. These results show that the time relaxation of the PPC effect is very similar to that of other metastable conditions in *a*-Si:H and supports the idea that the effect is simply produced by changes in the defect structure of *a*-Si:H, rather than by exotic trapping centers.

C. Numerical calculations

In this section we present results on calculations of the coplanar conductivity and the magnitude of the PPC effect in a doping-modulated *a*-Si:H multilayer as a function of sublayer thickness d , and compare them with experimental results. A variety of experimental techniques have been used to explore the different features of the gap-state distribution of *a*-Si:H.⁵³ Here we adopt the simplified representation of the density of states shown in Fig. 5. The band gap is taken to be 1.9 eV wide, which is close to the measured optical gap in our films, and the zero of energy is chosen at the midgap point. The conduction- and valence-band-tail densities of states $t_1(\epsilon)$ and $t_2(\epsilon)$, respectively, are of the form

$$t_1(\epsilon) = c_1 \exp\left[\frac{\epsilon}{\epsilon_1}\right], \quad (4a)$$

$$t_2(\epsilon) = c_2 \exp\left[\frac{-\epsilon}{\epsilon_2}\right], \quad (4b)$$

with characteristic energy slopes^{54,55} $\epsilon_1=22 \text{ meV}$ and $\epsilon_2=43 \text{ meV}$. The conduction-band tail has a linear energy dependence between 0.8 and 0.9 eV above midgap.⁵⁶

The Si dangling bond is believed to be the main defect in *a*-Si:H responsible for a broad maximum in the density of states near midgap.⁵⁷ A Si dangling bond can be found in three different charge states: neutral when occupied by

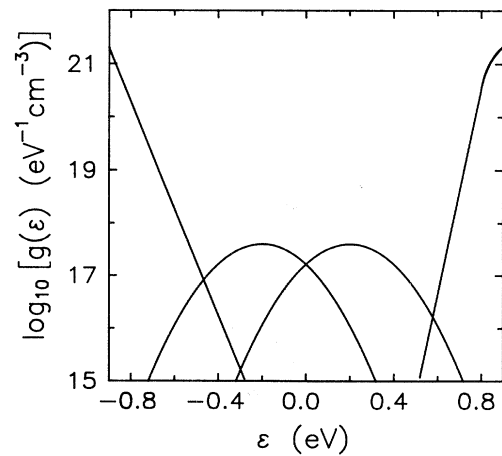


FIG. 5. Density of gap states used in the numerical calculations.

only one electron (D^0), positively charged when empty (D^+), and negatively charged when doubly occupied (D^-). Spin-resonance experiments have indicated that these states have a correlation energy of about 0.35 eV (Ref. 58) and hence there might be a distinct minimum in the density of states between D^0 and D^- when the Fermi level is near midgap. Deep level transient-spectroscopy measurements in n -type a -Si:H films find the width of the D^- peak to be about 0.15 eV.⁵⁹ Keeping these facts in mind, we model the defect density near midgap by the Gaussians

$$d_1(\varepsilon) = \frac{(N/2)}{\sqrt{2\pi}s} \exp\left[-\frac{(\varepsilon - \varepsilon_a)^2}{2s^2}\right], \quad (5a)$$

$$d_2(\varepsilon) = \frac{(N/2)}{\sqrt{2\pi}s} \exp\left[-\frac{(\varepsilon - \varepsilon_b)^2}{2s^2}\right], \quad (5b)$$

where $\varepsilon_a = 0.2$ eV, $\varepsilon_b = -0.2$ eV, $s = 0.15$ eV, and N , the number of gap defects, will be given different values N_n and N_p in the n - and p -type regions of the multilayer, respectively.

The states described by $t_1(\varepsilon)$ and $d_1(\varepsilon)$ are assumed to be acceptorlike states, in the sense that they are neutral when empty and can become negatively charged by accepting one electron. On the other hand, $t_2(\varepsilon)$ and $d_2(\varepsilon)$ are considered donorlike states: they are neutral when occupied by one electron and positively charged when empty. No state can be doubly occupied and no correlation effects are taken into account.

Thus, in this simplified model of the density of gap states, we use the one-electron-state distributions $d_1(\varepsilon)$ and $d_2(\varepsilon)$ to approximate a distribution of dangling bonds having a positive correlation energy, and we use the Fermi distribution function to determine the occupancy of the states instead of the proper partition function for correlated defects which can have 0, 1, and 2 occupancy. The main conclusions reached at the end of this section are independent of the details of the defect structure, and so the use of the above approximations is justified.

When a p - n junction is formed, electrons flow from the n -layer into the p -layer and bending of the bands takes place. The process of net charge transfer continues until a single equilibrium Fermi level ε_F describes the system, at which point the electron drift and diffusion currents cancel each other. The space charge density is then time independent and the problem can be treated electrostatically.

Let us consider a p - n - p - n . . . -type multilayer of sub-layer thickness d , and let x be the coordinate perpendicular to the junctions. We choose $x=0$ at the interface point of a p - n junction. Thus, to find the potential profile $V(x)$ of any single p - n junction and the position of ε_F we solve the system:

$$\frac{d^2}{dx^2} V(x) = \frac{e}{k\varepsilon_0} \rho(x), \quad (6)$$

$$\int_{-d/2}^{d/2} \rho(x) dx = 0, \quad (7)$$

subject to

$$V(x=0) = 0,$$

$$\left[\frac{dV}{dx}\right]_{-d/2} = \left[\frac{dV}{dx}\right]_{d/2} = 0.$$

Equation (6) is Poisson's equation and Eq. (7) expresses the condition of charge neutrality. In Eq. (6), e is the electronic charge and κ is the dielectric constant ($\kappa = 11$ for a -Si:H). The charge density $\rho(x)$ can be written as

$$\rho(x) = p(x) - n(x) + a(x) - b(x) + N_i(x). \quad (8)$$

Here $p(x)$ and $n(x)$ are the free-hole and free-electron densities, $a(x)$ and $b(x)$ are the charge densities in the acceptor and donorlike gap states, and $N_i(x)$ is the (signed) density of ionized dopants at position x . The free-carrier densities are given by

$$p(x) = p_0 \exp\{[\varepsilon_v + V(x) - \varepsilon_F]/kT\}, \quad (9)$$

$$n(x) = n_0 \exp\{[\varepsilon_F - V(x) - \varepsilon_c]/kT\}, \quad (10)$$

where ε_v , ε_c correspond to the valence-band and conduction-band mobility edge energies, T is the absolute temperature, and k is the Boltzmann factor.

The coefficients p_0 and n_0 are related to the conductivity prefactor through

$$\sigma_0 = n_0 e \mu_e \quad (11a)$$

for electron conduction and

$$\sigma_0 = p_0 e \mu_h \quad (11b)$$

for hole conduction, where μ_e and μ_h are the electron and hole mobilities. For $T = 300$ K we use $\mu_h = 1$ cm²V⁻¹s⁻¹, $\mu_e = 15$ cm²V⁻¹s⁻¹, and we take $\sigma_0 = 200$ Ω^{-1} cm⁻¹ as representative values for these quantities.^{54,59-64}

The quantities $a(x)$ and $b(x)$ in (8) are given by

$$a(x) = \int_{\varepsilon_v}^{\varepsilon_c} [t_1(\varepsilon) + d_1(\varepsilon)] f(\varepsilon + V(x)) d\varepsilon, \quad (12)$$

$$b(x) = \int_{\varepsilon_v}^{\varepsilon_c} [t_2(\varepsilon) + d_2(\varepsilon)] [1 - f(\varepsilon + V(x))] d\varepsilon, \quad (13)$$

where $f(\varepsilon)$ is the Fermi distribution function.

We will consider that all dopant atoms are ionized, which is an acceptable assumption as long as ε_F does not get too close (< 0.2 eV) to the band edges. Thus, $N_i(x)$ in Eq. (8) will simply be

$$N_i(x) = \begin{cases} -N_a, & -d < x < 0 \text{ (} p\text{-type layer)} \\ N_d, & 0 < x < d \text{ (} n\text{-type layer)} \end{cases}$$

where N_a and N_d are the densities of active acceptors and donors in the p - and n -type layers, respectively.

Once we know $V(x)$ and ε_F , the coplanar conductivity of the multilayer is calculated from

$$\sigma = \frac{1}{2d} \int_{-d}^d [\mu_e e n(x) + \mu_h e p(x)] dx. \quad (14)$$

Curves $A-E$ in Fig. 6 give the calculated dependence of the coplanar conductivity σ of a multilayer on layer thickness d for different choices of the parameters N_p ,

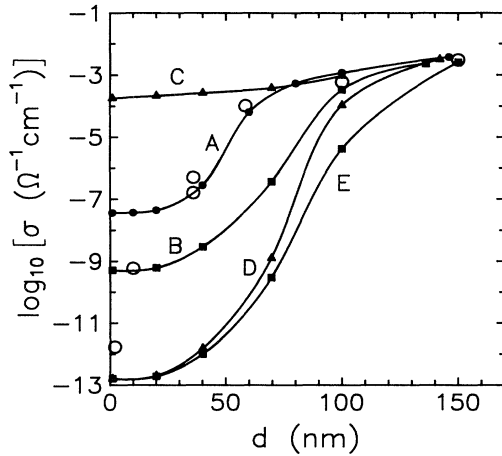


FIG. 6. Conductivity σ as a function of sublayer thickness d for p - n - p - n multilayer doped at 100 ppm. Open circles are experimental points. Closed symbols are calculated values. Solid lines are only a guide to the eye. The parameters used for curves A – E are given in Table III.

N_a , N_d . Table III specifies the value of these parameters for each curve.

Let us begin with curve A . The measured doping efficiency of a typical glow-discharge a -Si:H film doped at 100 ppm of phosphine (or diborane) in silane is about 0.06.⁶⁵ This means that, taking a density of Si atoms of $5.0 \times 10^{22} \text{ cm}^{-3}$, the number of active donors (fourfold-coordinated phosphorus atoms) in the film is $3.0 \times 10^{17} \text{ cm}^{-3}$. Thus, we choose N_d equal to this value. Next we find the value of the parameters N_n , N_a , and N_p that generate a best fit to the experimental values of the conductivity, measured in the annealed state at room temperature, with the restriction that at large d ($d > 150 \text{ nm}$) the coplanar conductivity of the multilayer must be close to the measured conductivity of the unlayered film n 100 (within a factor of 2). The result is curve A , with $N_a = 2.6 \times 10^{17} \text{ cm}^{-3}$ and $N_n = N_p = 5.0 \times 10^{16} \text{ cm}^{-3}$. The value $N_a = 2.6 \times 10^{17} \text{ cm}^{-3}$ corresponds to a doping efficiency of a little more than 0.05, which is within experimental error of the measured value of about 0.06,⁶⁵ while $N_n = N_p = 5.0 \times 10^{16} \text{ cm}^{-3}$ represent, as we will see in Sec. IV D, a compromise between the measured values of the number of dangling-bond defects N_{DB} at large d and

at small d (see Fig. 8). The closed symbols in Fig. 6 are calculated values, while the open circles are experimental points. The lines are drawn only as a guide to the eye. The agreement between curve A and the data points is very good for $d > 30 \text{ nm}$, but for $d < 10 \text{ nm}$ the measured σ values are several orders of magnitude smaller than the calculated ones. We shall comment on this discrepancy later.

In order to show the sensitivity of curve A to changes in the parameters, we also present in Fig. 6 a representative sample of other calculated curves. Each of the curves B – E in Fig. 6 is obtained from curve A by changing one of the parameters N_d , N_n , N_a , N_p at a time, as indicated in Table III.

The following points can be made from the results of these calculations. Within the approximations and restrictions we have adopted, there is a physically reasonable range of values for the parameters (N_d , N_n , N_a , N_p) that allow our calculations to reproduce the measured dependence of the coplanar conductivity of our multilayers (doped at 100 ppm) on sublayer thickness d , except for $d < 20 \text{ nm}$. The disagreement observed at $d < 20 \text{ nm}$ suggests that the regions of the multilayers carrying the coplanar current at small d have a different defect structure and perhaps carrier concentrations than those carrying it at large d . In fact, the only way for the calculated curves to agree with the data points over the complete range of sublayer thicknesses would be to allow the parameters to depend on d in the interval $0 < d < 20 \text{ nm}$ (see Sec. V).

It is also of interest to mention that the calculated conductivity curves become only weakly dependent on d for $d < 20 \text{ nm}$. This is so because at small d the height of the potential barrier at the p - n interfaces becomes at most only a few tens of meV, and further decrease of this barrier with decreasing d produces only a minor increase in the distance between the band edges and the equilibrium Fermi level. The fact that the experimental data points fall as steeply as they do at small d suggests again a changing defect structure and/or carrier concentration in the conducting regions of the multilayer with decreasing d in the range $0 < d < 20 \text{ nm}$.

We proceed now to calculate the magnitude of the PPC effect as a function of sublayer thickness for multilayers having the density of states used for curve A in Fig. 6 (see parameters in Table III). We assume that illumination generates in the p -type layers an additional concentration of dangling bonds having the Gaussian distribution

TABLE III. Parameter values for curves A – E in Fig. 9.

Curve	N_d (cm^{-3})	N_n (cm^{-3})	N_a (cm^{-3})	N_p (cm^{-3})
A	3.0×10^{17}	5.0×10^{16}	2.6×10^{17}	5.0×10^{16}
B	3.0×10^{17}	1.0×10^{17}	2.6×10^{17}	5.0×10^{16}
C	3.0×10^{17}	5.0×10^{16}	2.6×10^{17}	2.0×10^{16}
D	3.0×10^{17}	5.0×10^{16}	3.0×10^{17}	5.0×10^{16}
E	2.6×10^{17}	5.0×10^{16}	2.6×10^{17}	5.0×10^{16}

$$d_{\text{SW}}(\varepsilon) = \frac{N_{\text{SW}}}{\sqrt{2\pi a}} \exp\left[\frac{(\varepsilon - \varepsilon_{\text{SW}})^2}{2a^2}\right], \quad (15)$$

where the energies are measured from the midgap point of the p -type layer. We treat these dangling bonds as donorlike states in the sense explained earlier in this section. For an exposure time t_e of, say, 100s, we choose $N_{\text{SW}} = 5.0 \times 10^{16} \text{ cm}^{-3}$ and $a = 0.10 \text{ eV}$. We then adjust the value of ε_{SW} so that at $d = 36 \text{ nm}$ the value of the conductivity is ≈ 600 times larger than in the absence of the Staebler-Wronski defects (i.e., when $N_{\text{SW}} = 0$), as observed experimentally (see Fig. 7). The result is $\varepsilon_{\text{SW}} = 0.35 \text{ eV}$. Finally, with the above values of the parameters N_{SW} , a , and ε_{SW} we calculate a new curve of conductivity as a function of sublayer thickness d . The ratio between this new curve and curve A in Fig. 6 produces the solid curve in Fig. 7. The dots in Fig. 7 are calculated values and the line is only a guide to the eye. The open symbols give experimental values of the ratio $\sigma_{\text{PPC}}/\sigma_a$ between the dark conductivity in the PPC state σ_{PPC} measured a few minutes after an illumination of a couple of minutes and the conductivity σ_a of the annealed state. The circles are our experimental points, and the squares were taken from the work of Kakalios and Fritzsche⁴ who used a light intensity of 50 mW/cm^2 . We see again that the agreement between calculated and experimental values is good except for $d < 20 \text{ nm}$. This conclusion is not altered if we vary the parameter N_{SW} between, say, 1.0×10^{16} and $1.0 \times 10^{17} \text{ cm}^{-3}$. Each value of N_{SW} produces, of course, a different value for ε_{SW} according to the criterion described above. The finite value of the PPC in the limit $d = 0$ predicted by the calculations in Fig. 7 simply reflects the fact that the conductivity of the multilayer in this limit depends significantly on the defect concentration in the p layers.

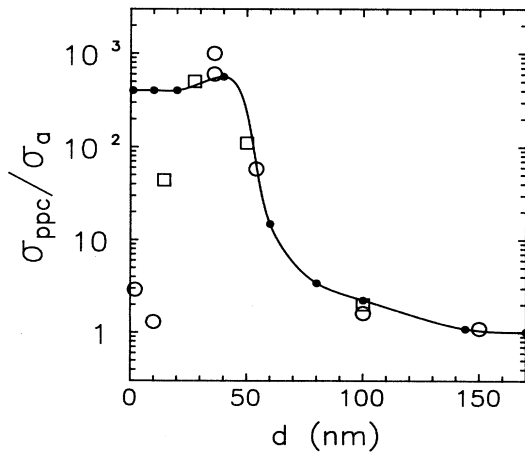


FIG. 7. Ratio between the conductivity σ_{PPC} in the PPC state and the conductivity σ_a of the annealed state. The dots are calculated values (see text). The line is only a guide to the eye. The open circles are our experimental values, while the squares are data from Ref. 4.

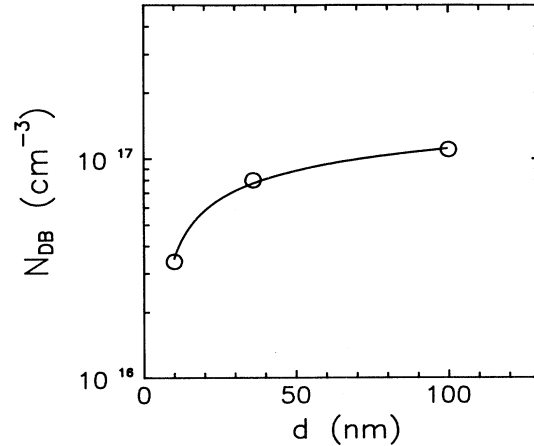


FIG. 8. Density of defects or dangling bonds N_{DB} obtained by photothermal deflection spectroscopy for multilayers $m1$, $m2$, and $m3$.

D. PDS data

The results in the previous section suggest that the average defect concentration and/or doping efficiency of the doped a -Si:H in the multilayer change with decreasing sublayer thickness d when $d < 20 \text{ nm}$. To test this proposition, we measured the density of dangling bonds N_{DB} in multilayers $m1$, $m2$, and $m3$, having $d = 100, 36$, and 10 nm respectively, using photothermal deflection spectroscopy (PDS).^{66–68}

Figure 8 presents our results. For $m3$, with $d = 100 \text{ nm}$, we obtain $N_{\text{DB}} = 1.2 \times 10^{17} \text{ cm}^{-3}$. This value lies between the PDS N_{DB} values obtained for single films $p100$ and $n100$, which are 5.0×10^{16} and $3.0 \times 10^{17} \text{ cm}^{-3}$, respectively. A slight decrease in defect density is observed in sample $m2$, having $d = 36 \text{ nm}$, for which $N_{\text{DB}} = 8.0 \times 10^{16} \text{ cm}^{-3}$. As we decrease further the sublayer thickness, a more dramatic drop in N_{DB} takes place. In multilayer $m3$, with $d = 10 \text{ nm}$, the value of N_{DB} is $3.3 \times 10^{16} \text{ cm}^{-3}$, three times smaller than in $m1$. We were unable to obtain N_{DB} for sample $m4$, having $d = 2 \text{ nm}$, because its total thickness of only 80 nm is not large enough to give a good and reliable PDS spectrum. We can say, however, that its N_{DB} value is even lower than that for $m3$. The PDS results show a clear trend: as d is decreased below a certain critical value, the defect density in the multilayer decreases with decreasing d .

E. PPC at small sublayer thickness

In this section we present results on the creation rate and annealing kinetics of the PPC in multilayers $m3$ and $m4$, having $d = 10$ and 2 nm , respectively. From the results in the previous two sections, we expect these samples not to follow the common behavior observed in multilayers having $d > 30 \text{ nm}$.

We see in Fig. 9 that *m3* and *m4* exhibit curves that resemble each other but look quite different from those we obtained for *m1* and *m2* (Fig. 2). In the case of *m4* there is a slow increase in σ_{PPC} for $t_e < 10^2$ s, which is followed by a more pronounced increase at longer exposures times. For $t_e = 10^5$ s, σ_{PPC} is about 300 times larger than σ_a in this sample. In the case of *m3* there is a small initial decrease in conductivity before a gradual but sustained increase with t_e takes over. It is interesting to note that even for $t_e = 10^5$ s the PPC effect has not completely saturated in samples *m3* and *m4*. This shows that the long exposures times ($t_e > 10^3$ s for light intensities of 50–100 mW/cm²) required to achieve saturation of the effect, which in the past were associated exclusively with compensated samples, can also be observed in multilayers.

The solid curves in Fig. 10 show the annealing cycles of the PPC state in samples *m3* and *m4* obtained after $t_e \approx 10^4$ s. We also include for comparison the annealing curve of the PPC state in *m2* after $t_e = 10^3$ s. The dashed lines show the annealing curves of the states obtained after $t_e = 10$ s. A coupling of points are noteworthy in Fig. 10. While the annealing temperature T_1 of the metastable excess conductance was 105°C for both *m1* and *m2*, we obtain $T_1 = 115$ and 140°C for *m3* and *m4*, respectively. Thus, T_1 appears to increase with decreasing d for values of d below a certain critical value. Something similar occurs with T_2 , the annealing temperature of the metastable decrease in conductivity. We obtained $T_2 = 160$ °C for *m1* and *m2*, but we get $T_2 = 180$ °C for *m3* and *m4*. We mention incidentally that the values for T_1 and T_2 are reproducible to within 3°C as one compares different annealing cycles of the same sample. A second point is that long exposure times ($t_e = 10^3$ s) are required to observe a metastable conductance decrease in the heating portion of the annealing cycles in samples *m1* and *m2*. This is not the case for samples *m3* and *m4*, as illustrated by the dashed lines in Fig. 10, obtained after $t_e = 10$ s.

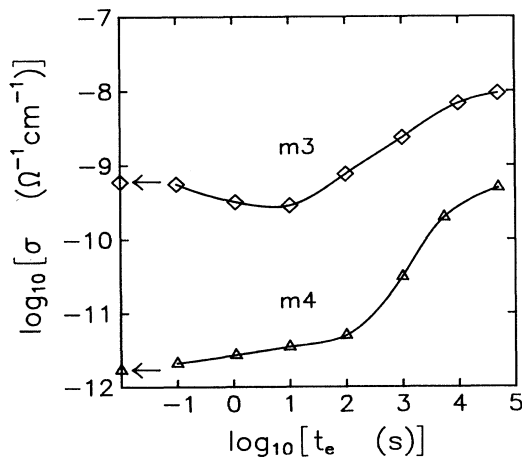


FIG. 9. Dark conductivity σ as a function of exposure time t_e at room temperature for multilayers *m3* and *m4*.

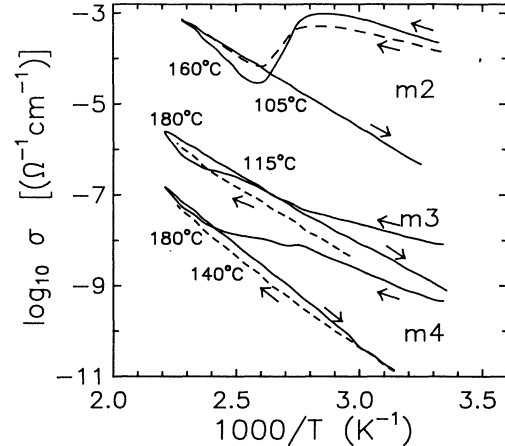


FIG. 10. Annealing curves of the PPC states in multilayers *m2*, *m3*, and *m4* obtained after $t_e = 10^3$ s (solid lines) and $t_e = 10$ s (dashed lines). The annealing temperatures T_1 of the excess conductance and T_2 of the conductance decrease are indicated for each curve.

It could be argued that sample *m4*, prepared in the form of a layered structure, is in fact a compensated film due to the interdiffusion of dopants across the 2-nm-thick sublayers during deposition. The substrate temperature was held at 220°C for about 55 min during the deposition of this sample. The first layer deposited remained then at the above temperature for 55 min, but the last layer only a few seconds, because the sample was cooled to room temperature at a rate of 6°C/min immediately after completing the last period.

Measurements of the diffusion coefficient D_B of boron for a *p*-type layer diffusing into undoped *a*-Si:H indicate that⁶⁹ $D_B = 10^{-18}$ cm²/s at 220°C, and recent results show that $D_B < 5 \times 10^{-18}$ cm²/s at 240°C for boron diffusing within a *p*-type film doped at 100 ppm.⁷⁰ If we assume a diffusion coefficient of 10^{-18} cm²/s for both phosphorus and boron atoms at 220°C, we can estimate the distance L the dopants diffuse by using $L = (Dt)^{1/2}$, where t denotes time. We find $L \approx 0.6$ nm in 55 min, or $L \approx 0.35$ nm in 20 min. Thus we expect most of the *a*-Si:H in the 2-nm-thick layers in sample *m4* to be singly doped, in particular in those periods deposited last.

As an additional test of whether interdiffusion of dopants is important for PPC we prepared a compensated sample, film *c1* in Table II, doped simultaneously with 100 ppm of phosphine and diborane in silane, and compare it with multilayer *m4*. As seen in Tables I and II, the activation energy and dark conductivity are very similar for both samples. However, unlike multilayer *m4*, the compensated film *c1* exhibited only a decrease in conduction when exposed to light for $t_e < 10^2$ s, and a very small PPC ($\sigma/\sigma_a \approx 2$) for $t_e > 10^2$ s. This small PPC almost disappeared after a 20-s etch in 25% HF, indicating that the effect was, at least in part, associated with the surface condition.²⁸ In multilayer *m4*, on the other hand, σ in-

creases by almost three orders of magnitude after $t_e \approx 10^5$ s, and this did not change after etching the sample.

Finally, in order to study the effect of the presence of a thin compensated region at the p - n interface on the properties of a multilayer, we prepared multilayer $m5$. This film has, like sample $m3$, a sublayer thickness $d = 10$ nm, but the last 2 nm of each layer were made of completely compensated material as described in Sec. II. The values of σ_a , E_a , and σ_p (see Table I) for sample $m5$, its response to light and annealing kinetics, were found to be undistinguishable from those observed in sample $m3$.

F. Unlayered films of various dopings

The results of the previous sections suggest that decreasing the sublayer thickness d of the p - n - p - n multilayer below a certain critical value produces a decrease in the density of dangling bonds and an increase in the annealing temperature of the light-induced metastable conductance changes. These trends are also observed in unlayered a -Si:H films of decreasing doping levels (see Sec. V). And in multilayers with small d , as in unlayered films of light doping levels, the Fermi level is positioned far from the band edges. We would then like to investigate whether or not the creation rate and annealing kinetics of the conductance changes in multilayers $m3$ and $m4$, having thin n -type and p -type layers prepared with a gas-phase doping of 100 ppm, can be consistently correlated with those that take place in unlayered p -type and n -type films of gas-phase doping levels smaller than 100 ppm, just as in Sec. IV A we correlated the behavior of multilayers $m1$ and $m2$ with that of unlayered films $p100$ and $n100$. With this purpose in mind we measured the creation rate and annealing temperature of the light-induced conductance changes in a series of unlayered a -Si:H films of decreasing doping level.

Figure 11 presents the light-induced decrease in conductance, or Staebler-Wronski effect, in p -type samples $p100$, $p10$, and $p1$ with gas-phase doping levels of 100,

10, and 1.0 ppm of diborane in silane, respectively. The arrows in Fig. 11 point to the values of the conductivity σ_a of the annealed state. We first notice in Fig. 11 that the initial (small t_e) response to light is fast at higher doping levels. Thus, at $t_e = 1$ s, for example, we find $\sigma/\sigma_a = 0.95$ for $p1$, 0.5 for $p10$, and 0.25 for $p100$. Second, while the decrease in conductivity has already saturated after $t_e = 10^2$ s for $p10$ and $p100$, the more lightly doped $p1$ shows a more gradual change that even at $t_e = 10^4$ s has not completely stopped. We notice in Fig. 11 that the total relative change in conductivity decreases with doping level from $p100$ to $p1$. These observations are valid for the range of doping levels of interest considered here. A heavily-boron-doped sample, 1% boron, for example, would show little change with light exposure. We also measured the temperature T_p at which the Staebler-Wronski defects disappear by annealing in these p -type samples, obtaining $T_p = 105$, 155, and 180°C for $p100$, $p10$, and $p1$, respectively.

The conductivity as a function of t_e for the n -type films is presented in Fig. 12. The gas-phase doping level of samples $n0.1$, $n1$, $n10$, and $n100$ is 0.1, 1.0, 10, and 100 ppm of phosphine in silane, respectively. The values of E_a in Table II reflect the motion of the Fermi level from being close to the center of the 1.8-eV a -Si:H gap in sample $n0.1$, to being close to the conduction band in sample $n100$. Figure 12 shows that for small t_e the response to light is faster for $n0.1$ the sample with the lower doping level. For $t_e = 10$ s, the conductivity has decreased by a factor of 5, while no significant change has yet occurred in the other samples. Secondly, the conductance changes have almost saturated in $n0.1$ after $t_e = 10^3$ s, when no signs of saturation are yet observable in the other samples. These two features are just the opposite of what we observed for the p -type films, where it was the more heavily doped sample $p100$ that exhibited a faster and larger response to light. The total relative change in conductivity is known to depend on a number of factors,

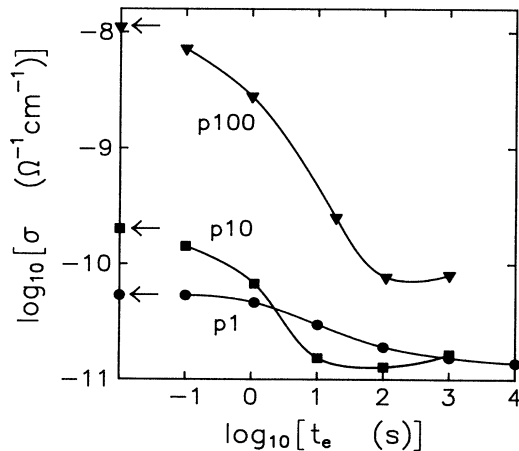


FIG. 11. Dark conductivity of boron-doped unlayered films $p1$, $p10$, and $p100$ as a function of exposure time t_e . Arrows indicate annealed values.

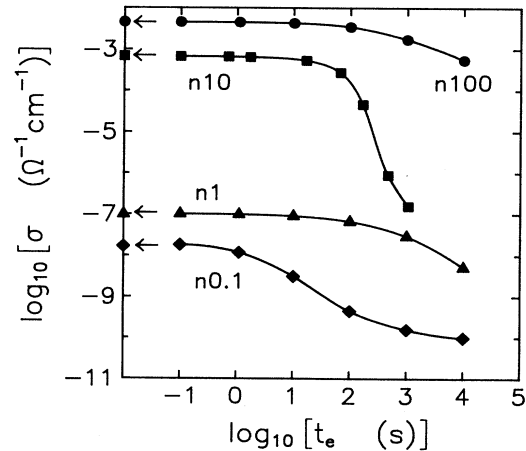


FIG. 12. Dark conductivity of phosphorus-doped unlayered films $n0.1$, $n1$, $n10$, and $n100$ as a function of exposure time t_e . Arrows indicate annealed values.

namely, the position of the Fermi level in the gap, the density of states at that energy, and the number of additional defects created by light. According to Fig. 12, these factors seem to produce a maximum change in conductivity for concentrations of donors similar to that in sample *n*10 (10 ppm PH₃). The annealing temperature T_n of the Staebler-Wronski defects in these *n*-type films increases, as before, with decreasing doping level, being $T_n = 150, 155, 180,$ and 190°C for samples *n*100, *n*10, *n*1, and *n*0.1, respectively. We mention here that all values for $T_1, T_2, T_p,$ and T_n given in this study are reproducible to $\pm 5^\circ\text{C}$ as one compares different samples having the same doping concentrations but prepared in different runs.

The results of this section show that the creation rate of the conductance changes in multilayers *m*3 and *m*4 (Fig. 9), having $d = 10$ and 2 nm, respectively, is consistent, at least qualitatively, with the rate in unlayered films of very small doping levels, like *p*1 and *n*0.1: the small exposures ($t_e < 10$ s) required to see a metastable de-

crease in conductance in the heating curves of samples *m*3 and *m*4 (Fig. 10) are consistent with the fast response to light observed in film *n*0.1, and the large exposures ($t_e > 10^3$ s) required to saturate the PPC effect in *m*3 and *m*4 are consistent with the slow saturation of the Staebler-Wronski defects in film *p*1. We will discuss in Sec. V why the observed behavior in multilayers with small d is just what one should have expected.

G. Compensated samples

Figure 13(a) shows the dark conductivity as a function of t_e for the partially compensated *n*-type film *c*2, doped with 53 ppm diborane and 530 ppm phosphine in silane (Table II). The curve is very similar to that we obtained in Fig. 10 for multilayer *m*4 ($d = 2\text{nm}$) in that there is a slow increase in σ for $t_e < 10^2$ s followed by a faster increase that tends to saturate only after $t_e \approx 10^5$ s.

The annealing curve of the PPC state obtained after $t_e \approx 10^5$ s is given in Fig. 13(b). In this case the PPC anneals at $T_1 = 120^\circ\text{C}$. The annealing temperature of the Staebler-Wronski defects in the corresponding unlayered *p*-type film, sample *p*53 doped at 53 ppm of diborane in silane, is $T_p = 90^\circ\text{C}$. Thus, we see in film *c*2, as in multilayers *m*3 and *m*4, that $T_1 > T_p$. No remnant decrease in conductance is observed in film *c*2 after the PPC has been eliminated by annealing. This observation is consistent with the low annealing point of the Staebler-Wronski defects in the unlayered *n*-type film *n*530, doped with 530 ppm of phosphine in silane, for which we measured $T_n = 90^\circ\text{C}$.

H. High-bias effects

In this section we make a brief digression to mention some high-bias anomalies that could lead one to misjudge the magnitude of the light-induced excess bulk conductance in the multilayers. Figure 14(a) shows the dark current in the annealed state (curve *A*) and the photocurrent (curve *B*) of sample *m*2 as a function of the voltage applied across the 2-mm gap Ni-Cr-covered Mg electrodes. Circles and squares in the figure refer to opposite polarities. The points on curve *B* are reproducible as one goes back and forth changing the voltage, which means that within the time span it takes to obtain the data points, the Staebler-Wronski defects created by illumination do not affect significantly the value of the photocurrent. It can be seen that while curve *A* exhibits an Ohmic behavior all the way to the highest applied voltage of 1000 V, curve *B* becomes sub-Ohmic above a few volts.

Figure 14(b) shows the current-voltage characteristic in two different PPC states (t_e, V_i), obtained after an exposure time t_e and applying a voltage *during* illumination V_i . Circles refer to positive polarity (same as V_i) and squares to negative polarity. We see that the I - V curve for the PPC state (100 s, 0 V) becomes strongly sub-Ohmic above $V = 1$ V, but the values obtained are independent of the polarity of the measuring voltage V . In fact, the same I - V curve is obtained for all PPC states (100 s, V_i) as long as $V_i < 10$ V. In other words, as long as V_i is the Ohmic regime of the photocurrent-voltage

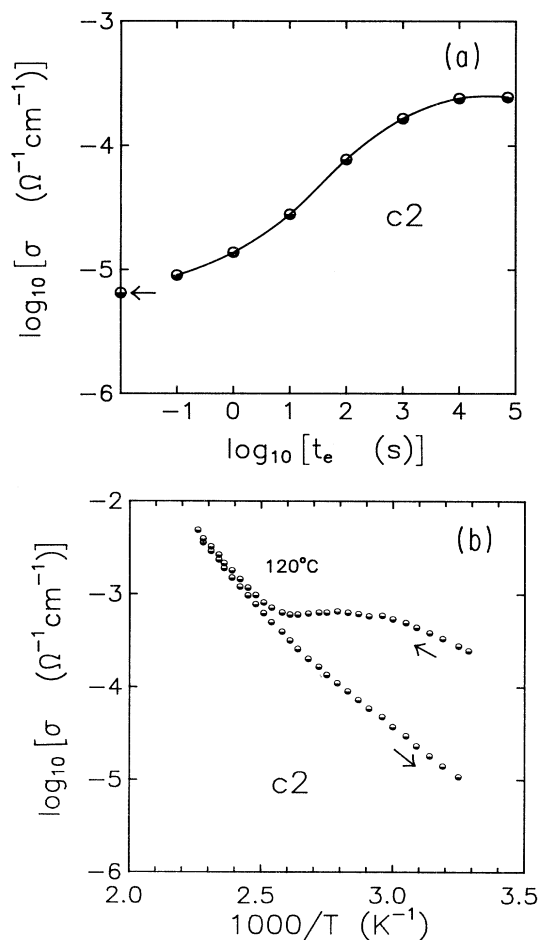


FIG. 13. (a) Dark conductivity as a function of exposure time for compensated film *c*2. The arrow indicates the annealed value. (b) Annealing curve of the PPC state in sample *c*2 after $t_e = 10^5$ s.

characteristic [curve *B* in Fig. 14(a)], the I - V curve of the resulting PPC state (100 s, V_i) is independent of the voltage V_i applied during illumination.

On the other hand, if V_i falls in the non-Ohmic regime of curve *B* in Fig. 14(a), then the I - V curve of the PPC state (100 s, V_i) exhibits certain anomalies that become more pronounced as V_i is made larger. For example, Fig. 14(b) also shows the I - V curve for the PPC state (100 s, 700 V). It is seen that there is a strong asymmetry with the change in polarity of the measuring voltage. While negative polarity gives an I - V characteristic similar to that of that state (100 s, 0 V), the positive polarity gives current values that are an order of magnitude smaller in most of the explored voltage range. A further important

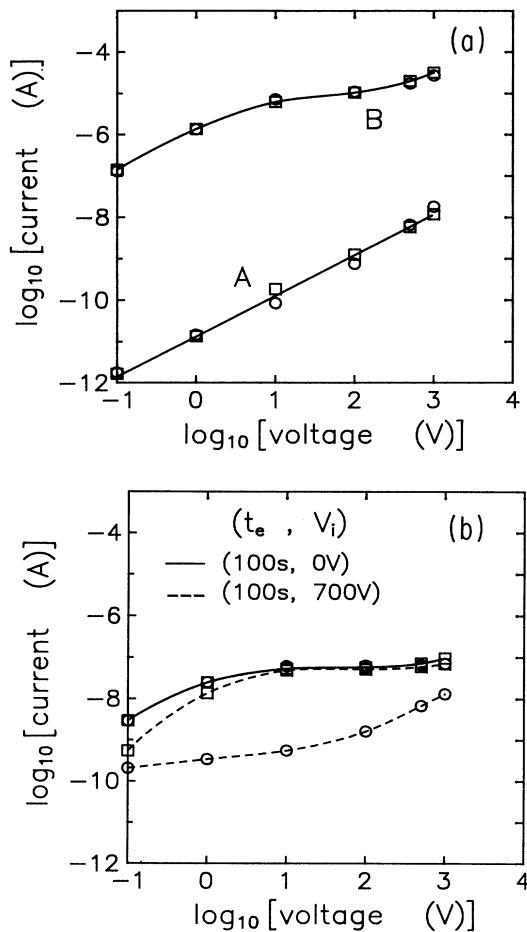


FIG. 14. (a) Current-voltage characteristic in the annealed state (curve *A*) and during illumination (curve *B*) for multilayer *m2*. Circles and squares correspond to opposite polarities of the measuring voltage V . (b) Dark current-voltage characteristic of sample *m2* in the PPC states (t_e , V_i), which are obtained by applying a voltage V_i during the time t_e that the sample is exposed to light. Circles correspond to positive polarity (same as V_i) of the measuring voltage V . Squares indicate negative polarity.

result is this: if one proceeds to illuminate the sample for another 5 s, but setting $V_i=0$, then one recovers the I - V curve obtained in the state (100 s, 0 V). This result shows that the lower current values obtained with positive polarity in the PPC state (100 s, 700 V) are not due to changes in the defect structure of the bulk of the multilayer, but rather to some charging effect taking place in the region near one of the electrodes.

V. DISCUSSION

A. Multilayers

Our model can satisfactorily explain all the experimental facts associated with the PPC in doping-modulated *a*-Si:H multilayers. The long decay times of the PPC at room temperature are explained by the long decay times of the Staebler-Wronski defects observed in *p*-type unlayered films. Furthermore, both the PPC and the metastable changes in the defect structure of unlayered *a*-Si:H are found to follow stretched-exponential time decays with similar parameters. The large magnitude of the PPC observed at room temperature can be obtained, as shown in Sec. IV C, by a number of Staebler-Wronski defects that do not seem too difficult to attain in a *p*-type unlayered *a*-Si:H film doped at 100 ppm at the light exposures involved.⁷¹ Our model is favored by the evidence of the defect-pool model,⁷²⁻⁷⁵ which places D^+ in *p*-type material well above midgap. The observed activated behavior for the creation of PPC (Refs. 10 and 14) can be understood within the model in terms of the temperature dependence of the efficiency for the creation of Staebler-Wronski defects in *p*-type and *n*-type materials.

According to the model, we do not expect to see PPC in *n-i-n-i* multilayers, because Staebler-Wronski defects are found to be created below the Fermi level both in *n*-type and undoped unlayered films, pulling the Fermi level in these films closer to midgap. Thus, the Fermi level in the multilayer can only move away from the conduction band in the *n* regions of the multilayer after illumination, producing a conductivity decrease. We do not expect to see PPC in *p*-type *p-i-p-i* multilayers either, because the faster and larger response to light observed in *p* type unlayered films should make the *p* regions of the multilayer more intrinsic before the undoped regions, shifting the Fermi level of the multilayer away from the valence band and closer to midgap, thereby decreasing the conductivity. Thus, in both kinds of multilayers a decrease in conductance is expected rather than the PPC effect, and in agreement with the predictions of the model no PPC has been observed in these multilayers.^{8,76}

The role of the internal junction fields and the question of the apparent low quantum efficiency in the creation of PPC are discussed in Sec. V C. In Sec. IV C we saw that quantitative agreement between calculated and experimental values of the conductivity and the magnitude of the PPC in multilayers with small d can be achieved if we assume a changing defect structure and doping efficiency in the *p*-type and *n*-type regions with decreasing d , for $d < 20$ nm. In the following section we discuss this matter in more detail.

B. Multilayers with small d

We discuss now our results for multilayers with small sublayer thickness d . It is useful to begin by reviewing some relevant facts on unlayered a -Si:H films. Experimental results suggest that the position of the Fermi level within the mobility gap of the semiconductor determines, at least in part, the density of dangling bonds and the doping efficiency (defined here as the fraction of dopant atoms that are active). The defect density is found to increase with increasing doping level in singly doped films, but not in compensated samples.^{77–79} In the first case, the Fermi level gets closer to the band edges, while in the second it remains near midgap. This fact suggests that the defect creation process is the result of the shift of the Fermi level rather than some disordering effect due to the dopant atoms, and is one of the basic elements of the doping model for a -Si:H.^{57,80} The application of high biases that create carrier accumulation regions and bring the Fermi level closer to one of the band edges has also been shown to increase the defect density in a -Si:H.⁴⁴ The doping efficiency, on the other hand, increases with decreasing doping level.⁶⁵ Experimental results also indicate that application of a depletion bias in an a -Si:H Schottky-barrier structure depresses the Fermi energy and increases the fraction of active donors in the phosphorus-doped layer.^{59,81} Another consideration is that the annealing temperature of the metastable changes in the defect structure of a -Si:H decreases with increasing doping level in singly doped films, as found in Sec. IV F, but not in compensated samples. Again, one could argue that the annealing temperature is determined, at least in part, by the position of the Fermi level and the resulting defect structure. In the hydrogen glass model for a -Si:H (Refs. 44 and 52) one expects the annealing temperature to be lower when the hydrogen diffusion coefficient in the film is higher. Studies in singly doped and compensated films show that this coefficient increases with increasing concentration of dangling bonds.⁷⁰ Finally, Figs. 11 and 12 suggest the unsurprising result that the relative magnitude of the light-induced changes in the defect density and the exposure required for saturation depend on the position of the Fermi level and the details of the defect structure.

A multilayer with sublayer thickness d larger than the depletion lengths in the p - and n -type regions will contain bulk or nondepleted zones in addition to the depletion zones. In this case the height of the potential barriers at the p - n interfaces is equal to mismatch between the Fermi levels of the corresponding unlayered p - and n -type films. In the bulk zones, and in those portions of the depletion zones close to them, the position of the Fermi level in relation to the band edges, the gap defect density, and the carriers concentrations are the same as those in the corresponding unlayered films. As one moves away from a bulk zone, deeper into the depletion zone, the distance between the Fermi level and the corresponding band edge (conduction band in n -type regions, valence band in p -type regions) increases due to the bending of the bands and reaches a maximum at the p - n interface. In view of our previous discussion, we would then expect the de-

pletion zone to have a lower concentration of dangling bonds, a higher doping efficiency, a different response to light and a higher value of the annealing temperature than the bulk zone. For a given light exposure, the conductance changes in the multilayer are dominated by the Staebler-Wronski defects created either in the bulk or in the depletion zones.

As the sublayer thickness d of the multilayer is decreased below the values of the depletion lengths, the height of the potential barriers at the p - n junctions decreases and a smaller portion of the depletion zones, adjacent to the p - n interfaces, remains. The p - and n -type regions are then more intrinsiclike and the following trends in the properties of the multilayers are observed, as expected. The PDS results in Sec. IV D clearly show that the defect density decreases with decreasing d . The results in Sec. IV C indicate that the steep decrease in σ_a for multilayers with $d < 20$ nm can be explained, for example, if a slightly higher (5–10%) value of boron-doping efficiency exists in the corresponding portion of the depletion zones (compare curves A and D in Fig. 6). It is likely that there is also a higher phosphorus-doping efficiency, but the increase in active boron dopants must be proportionally larger in order to explain the observed decrease in σ_a . More generally, the combined effect of the changing defect densities and doping efficiencies in the p - and n -type regions of the multilayer with decreasing d must lead to the observed steep decrease in σ_a . The annealing curves in Fig. 10 show how the temperatures T_1 and T_2 increase with decreasing d , as expected.

Alternatively, the different behaviors observed between multilayers of thin and thick sublayer thickness d could be attributed to different microstructures of the doped sublayers. The microstructure, associated with either the hydrogen content or doping, of very thin a -Si:H films may be very different from that of thicker samples. If, for example, a change in microstructure with decreasing sublayer thickness causes the hydrogen diffusion coefficient in the sublayer to decrease, then we would expect the annealing temperature of the PPC effect to increase with decreasing d , as observed.

C. Internal fields and microscopic reactions

It could be argued that the changes in the defect structure of the p -type regions, responsible for the PPC in our n -type multilayers, are not brought about by the photo-generated excess concentrations of band-tail carriers that will eventually recombine, but rather by that small fraction of photogenerated holes that are moved from the n -type regions into the p -type regions by the internal fields. The arguments presented below suggest that this is not the case, and that it is indeed the excess concentration of carriers generated directly by light in the p -type regions, and/or the subsequent recombination of these carriers, that determines to what extent the defect structure of these regions is altered.

In a multilayer like sample $m2$, having a sublayer thickness of 36 nm, the space charge N_Q on each side of a p - n junction in the dark and the associated electric field E

at the p - n interface can be estimated to be $N_Q \approx 10^{18}$ e/cm^3 and $E \approx 10^5$ V/cm. The drift length of a carrier in this field at room temperature is several tens of nanometers.² Thus, immediately after turning the light on, electrons and holes photoexcited near the p - n interface are moved into the n -type and p -type regions, respectively, by the internal field before they have a chance to recombine. These separated charges decrease in turn the magnitude of the field, and the process continues until the carrier drift length is not large enough to keep the photoexcited electron-hole pairs from recombining. The maximum number of charges that can be separated before this process stops is N_Q . For a light intensity from our light source of $I = 1$ mW/cm², which corresponds to a photon flux of about 5.0×10^{19} photon/s cm³, it takes then only $t_s \approx 20$ ms to neutralize the internal fields. Increasing the light intensity by two orders of magnitude, for example, will decrease t_s and increase the number of recombination processes (per unit time) by two orders of magnitude as well, but the number of holes and electrons that have been moved into the p -type and n -type regions after a time t_s is still the same. Thus, if these separated holes are responsible for the changes in the defect structure of the p -type regions that produce the PPC, the same magnitude of the PPC effect should occur when we expose the sample $m2$ to light during, say, $t_e = 100$ s using $I = 1$ mW/cm² or $I = 100$ mW/cm². We have observed, however, that the magnitude of the PPC is an order of magnitude smaller when using $I = 1$ mW/cm². The dependence of the PPC on light intensity has been measured before.¹⁰ The above experimental fact, together with the close correlation observed between the rate of creation of defects in the boron-doped film $p100$ and the rate of creation of PPC in multilayers $m1$ and $m2$ for a given light intensity (see Fig. 2), leads us to believe that the changes produced in the p -type regions of the multilayers are induced by the photocarriers generated mainly in the p -type regions.

The microscopic mechanism by which light creates additional defects in the gap of a boron-doped a -Si:H film is still unclear. It has been proposed that the energy released in recombination processes allows the breaking of weak silicon—silicon bonds.³⁰ Defects in a -Si:H can also be created by other means (see Sec. IV B), single-carrier injection, for example, but it is not clear that the microscopic reactions responsible for the creation of additional defects are the same in all cases.

Recent experiments in compensated films using Schottky-barrier structures have shown that single-carrier injection can also produce PPC in these films.²⁴ It is found that hole injection is only slightly less efficient in producing PPC than band-gap illumination, but electron injection is considerably less efficient in producing the effect.²⁴ It is thus possible that excess holes create defects in boron-doped films more efficiently than excess electrons. Experiments in undoped a -Si:H show that the conductivity can be decreased significantly by hole injection, but not by electron injection.³⁶ It is then possible that defects created by light in the p -type regions are associated both with recombination processes and with the light-induced excess concentration of holes.

D. Transverse PPC

The PPC effect has also been observed in the conductance perpendicular to the layers of doping-modulated a -Si:H multilayers.¹⁵ The transverse conduction of an n -type p - n - p - n multilayer may take place by electron hopping through the localized states in the p -type layers⁴⁵ or through conduction-band extended states over the potential barriers.⁴⁵ The hopping current is seen to dominate at low measuring biases, while band conduction dominates at high measuring biases. In the PPC state of a multilayer, both hopping and band currents are seen to increase.¹⁵

The existence of a transverse PPC can be explained as follows. Light creates additional defects above the Fermi level in the p -type layers, while no significant change in the defect structure of the n -type layers has yet occurred. This increases the number of hopping centers and thus the hopping current. The new position of the Fermi level in the multilayer, closer to the conduction band, implies a larger concentration of band-tail electrons in the n -type regions and a consequent increase in the band current. If the Fermi level has moved into a region of larger density of defects in the p -type regions, then there will also be a contribution to the hopping current due to the shift of the Fermi level.

E. Compensated films

The idea of a common origin for the PPC in multilayers and compensated films has been suggested in the past.^{8,13} We already mentioned in Sec. IV G the similarities between the creation rate and annealing kinetics observed in compensated film $c2$ and multilayer $m4$, which has a small sublayer thickness ($d = 2$ nm). It is also known that, as in multilayers, only n -type or slightly p -type compensated films exhibit PPC.

We believe that a compensated film, such as $c2$, can be considered an aggregate of small (a few nm) p -type and n -type regions rather than a material where the dopant atoms are homogeneously distributed. Then our model to explain PPC in multilayers can be extended to compensated films, either if conduction in the compensated material takes place through percolation paths in the n -type regions or by electron hopping and band conduction across the p -type regions.

We must point out that the magnitude of random charge fluctuations is not enough to produce p -type regions in an otherwise homogeneous compensated sample doped with 530 ppm phosphine and 53 ppm diborane. However, boron doping is known to produce compositional and structural inhomogeneities in the bulk of a -Si:H.^{82,83} We notice that, just like very thin layers in a p - n multilayer, the small p -type and n -type regions in the aggregate are depleted and thus more intrinsiclike and then, according to our discussion in Sec. V B, are expected to have a lower defect density, and perhaps a different doping efficiency, than bulk or nondepleted material of the same doping level.

F. A more general version

We would like to rephrase our model in more general terms to explain the conductance changes induced by light (or by other means) in modulated multilayers (p - n - p - n , p - i - p - i , n - i - n - i , n - i - p - i) and compensated films, as follows. Our model assumes that light creates Staebler-Wronski defects in the p - and n -type regions of the composite material, changing their localized gap-state distribution and, in particular, making them more intrinsic. The potential profile of the depletion regions depends on the local defect structure and carrier concentrations in the p - and n -type regions. Thus, after exposing the composite film to light, the energy distance between the Fermi level and the band edges will change in the depletion and bulk zones (if any) of the composite film. This will generate a change in conductance whose direction and magnitude are determined by the initial (before illumination) position of the Fermi level and the magnitude and rate of the relative changes induced by light in the defect structure of the p -type and n -type regions.

G. Other models for PPC

As indicated in the Introduction, previous models proposed to explain the PPC effect in doping-modulated and compensated a -Si:H can be grouped into those that invoke the existence of a novel hole-trapping center, and the one more recently put forward by Kakalios and Street that explains the effect in terms of the thermal equilibration model for a -Si:H. In the model of Kakalios and Street, like in ours, the effect is produced by metastable changes induced during illumination in the defect structure of the p -type regions. These changes, which could affect the defect concentration and/or doping efficiency, are, however, said to be brought about by that small fraction of photogenerated holes that are moved from the n -type regions into the p -type regions by the internal fields. We believe this model can also explain, for example, all the experimental facts referred to in Sec. V A. We do not understand in terms of this model, though, the dependence of the magnitude of the PPC on light intensity as discussed in Sec. V C, and the close correlation that for a given light intensity one obtains between the conductance changes as a function of exposure time in the multilayers and in unlayered p -type and n -type films as presented in Sec. IV A.

Models postulating the existence of a novel trapping center can also eventually explain the experimental results if one assigns to this center the right set of properties. This demands a number of additional assumptions, which, we believe, are unnecessary as long as there is available a simpler model able to explain the PPC in

terms of another well-known effect in a -Si:H, namely, the Staebler-Wronski effect.

VI. SUMMARY AND CONCLUSIONS

We summarize our conclusions in the following points.

(1) The PPC effect in a -Si:H p - n multilayers and compensated films can be explained in terms of the Staebler-Wronski defects created directly by light in the p -type regions of the material. No exotic hole-trapping centers are required to account for the excess electronic current in the PPC state.

(2) The microscopic reactions leading to the generation of additional defects by light in the gap of the p -type and n -type materials are expected to be the same either if these materials are unlayered or incorporated in a composite. Thus we expect the main microscopic reaction responsible for the PPC effect to involve the creation of dangling bonds.

(3) The role of the p - n -junction fields in the production of the PPC effect is a minor one. Our results suggest that, for the light intensities typically used to produce PPC, the effect is mainly due to the excess carrier concentrations generated by light (and/or subsequent recombination processes) rather than to the field-separated photocarriers.

(4) Our results indicate that the depletion zones of a multilayer, where the Fermi level lies closer to midgap, have a lower concentration of defects, and perhaps a higher doping efficiency, than the bulk or nondepleted zones. This is in agreement with previous studies in a -Si:H that indicate that the position of the Fermi level within the gap of the semiconductor influences the details of the defect structure.

(5) Light-induced conductance changes in other a -Si:H layered structures, like n - i - n - i , p - i - p - i , and n - i - p - i multilayers, can also be explained in terms of the Staebler-Wronski defects created in the different layers and the resultant new energy distance between the Fermi level and the band edges throughout the structure.

ACKNOWLEDGMENTS

I would like to express by deepest gratitude to my Ph.D. thesis advisor, Professor Hellmut Fritzsche, from whose knowledge, physical insight, and constant advice I benefited greatly throughout the period of my graduate studies at The University of Chicago. This work was partially supported by NSF DMR-8806197 and by the Material Research Laboratory at The University of Chicago supported by the National Science Foundation. I would like to thank the Eileen S. Andrew Foundation for partial support for three consecutive years.

¹H. Mell and W. Beyer, *J. Non-Cryst. Solids* **59&60**, 405 (1983).

²J. Kakalios and H. Fritzsche, *Phys. Rev. Lett.* **53**, 1602 (1984).

³J. Kakalios and H. Fritzsche, *J. Non-Cryst. Solids* **77&78**, 1101 (1985).

⁴J. Kakalios and H. Fritzsche, in *Layered Structures, Epitaxy, and Interfaces*, edited by J. M. Gibson and L. R. Dawson, MRS Symposia Proceedings No. 37 (Materials Research So-

ciety, New York, 1985), p. 29.

⁵I. Chen, *Phys. Rev. B* **32**, 879 (1985).

⁶F. C. Su, S. Levine, P. E. Vanier, and F. J. Kampas, *Appl. Phys. Lett.* **47**, 612 (1985).

⁷M. Hundhausen and L. Ley, *Phys. Rev. B* **32**, 6655 (1985).

⁸S. C. Agarwal and S. Guha, *Phys. Rev. B* **32**, 8469 (1985).

⁹S. C. Agarwal and S. Guha, *J. Non-Cryst. Solids* **77&78**, 1097

- (1985).
- ¹⁰J. Kakalios, *Philos. Mag. B* **54**, 199 (1986).
- ¹¹I. Chen, *Phys. Rev. B* **33**, 8433 (1986).
- ¹²S. H. Choi, B. S. Yoo, C. Lee, and J. Jang, *Phys. Rev. B* **36**, 6479 (1987).
- ¹³J. Kakalios and R. A. Street, in *Disordered Semiconductors*, edited by M. A. Kastner, G. A. Thomas, and S. R. Ovshinsky (Plenum, New York, 1987), p. 529.
- ¹⁴A. Vomvas and H. Fritzsche, *Philos. Mag. Lett.* **56**, 197 (1987).
- ¹⁵J. Takada and H. Fritzsche, *J. Non-Cryst. Solids* **97&98**, 907 (1987).
- ¹⁶B. S. Yoo, S. H. Choi, C. Lee, and J. Jang, *Superlatt. Microstruct.* **4**, 133 (1988).
- ¹⁷D. H. Zhang and D. Haneman, *J. Appl. Phys.* **63**, 1591 (1988).
- ¹⁸D. H. Zhang and D. Haneman, *Appl. Phys. Lett.* **52**, 1392 (1988).
- ¹⁹H. Ito and M. Kikuchi, *Jpn. J. Appl. Phys.* **27**, 1787 (1988).
- ²⁰J. Jang, S. C. Kim, and C. Lee, *J. Appl. Phys.* **64**, 6583 (1988).
- ²¹A. Hamed and H. Fritzsche, *Philos. Mag. Lett.* **60**, 171 (1989).
- ²²J. Kakalios, *J. Non-Cryst. Solids* **114**, 714 (1989).
- ²³A. Hamed and H. Fritzsche, *J. Non-Cryst. Solids* **114**, 717 (1989).
- ²⁴B. S. Yoo, Y. H. Song, C. Lee, and J. Jang, *Phys. Rev. B* **41**, 10787 (1990).
- ²⁵A. Hamed and H. Fritzsche, *Philos. Mag. B* **63**, 33 (1991).
- ²⁶G. H. Doler, H. Kunzel, and K. Plogg, *Phys. Rev. B* **25**, 2616 (1982).
- ²⁷D. L. Staebler and C. R. Wronski, *Appl. Phys. Lett.* **31**, 292 (1977); *J. Appl. Phys.* **51**, 3262 (1980).
- ²⁸B. Aker and H. Fritzsche, *J. Appl. Phys.* **54**, 6628 (1983).
- ²⁹M. Tanielian, *Philos. Mag. B* **45**, 435 (1982).
- ³⁰M. Stutzmann, W. B. Jackson, and C. C. Tsai, *Phys. Rev. B* **32**, 23 (1985).
- ³¹E. Eser, *J. Appl. Phys.* **59**, 3508 (1986).
- ³²X. M. Deng and H. Fritzsche, *Phys. Rev. B* **36**, 9378 (1987).
- ³³D. Redfield, *Appl. Phys. Lett.* **48**, 846 (1986).
- ³⁴D. L. Staebler, R. S. Crandall, and R. Williams, *Appl. Phys. Lett.* **39**, 733 (1981).
- ³⁵H. Pfeleiderer, K. Kusian, and W. Kruhler, *Solid State Commun.* **49**, 493 (1984).
- ³⁶W. Kruhler, H. Pfeleiderer, R. Plattner, and W. Stetter, in *Optical Effects in Amorphous Semiconductors*, Proceedings of the International Topical Conference on Optical Effects in Amorphous Semiconductors, AIP Conf. Proc. No. 120, edited by P. C. Taylor and S. G. Bishop (AIP, New York, 1984), p. 311.
- ³⁷R. A. Street, J. Kakalios, C. C. Tasi, and T. M. Hayes, *Phys. Rev. B* **35**, 1316 (1987).
- ³⁸J. Kakalios, R. A. Street, and W. B. Jackson, *Phys. Rev. Lett.* **59**, 1037 (1987).
- ³⁹J. Kakalios and R. A. Street, in *Advances in Amorphous Semiconductors: Amorphous Silicon and Related Materials*, edited by H. Fritzsche (World Scientific, Singapore, 1989), Vol. 1, p. 615.
- ⁴⁰Y. H. Song, B. S. Yoo, C. Lee, and J. Jang, *J. Non-Cryst. Solids* **114**, 666 (1989).
- ⁴¹J. Takada and H. Fritzsche, *J. Non-Cryst. Solids* **97&98**, 907 (1987).
- ⁴²S. H. Choi, B. S. Yoo, C. Lee, and J. Jang, *J. Non-Cryst. Solids* **97&98**, 1001 (1987).
- ⁴³H. Fritzsche, S. H. Yang, and J. Takada, in *Amorphous Silicon Technology*, edited by A. Madan, M. J. Thompson, P. C. Taylor, P. G. LeComber, and Y. Hamakawa, MRS Symposia Proceedings No. 118 (Materials Research Society, Pittsburgh, 1988), p. 275.
- ⁴⁴W. B. Jackson and J. Kakalios, in *Advances in Amorphous Semiconductors: Amorphous Silicon and Related Materials* (Ref. 39), p. 247.
- ⁴⁵B. S. Yoo, Y. H. Song, C. Lee, and J. Jang, *Superlatt. Microstruct.* **5**, 153 (1989); *Phys. Rev. B* **39**, 11050 (1989).
- ⁴⁶D. V. Lang, J. D. Cohen, and J. P. Harbison, *Phys. Rev. Lett.* **48**, 421 (1982).
- ⁴⁷A. R. Hepburn, J. M. Marshall, C. Main, M. J. Powell, and C. van Berkel, *Phys. Rev. Lett.* **56**, 2215 (1986); A. R. Hepburn, C. Main, J. M. Marshall, C. van Berkel, and M. J. Powell, *J. Non-Cryst. Solids* **97&98**, 903 (1987).
- ⁴⁸W. B. Jackson and D. M. Moyer, *Phys. Rev. B* **36**, 6217 (1987).
- ⁴⁹R. E. I. Schropp and J. F. Verwey, *Appl. Phys. Lett.* **50**, 185 (1987).
- ⁵⁰R. E. I. Schropp, A. J. Boonstra, and T. M. Klapwijk, *J. Non-Cryst. Solids* **97&98**, 1339 (1987).
- ⁵¹W. B. Jackson and J. Kakalios, *Phys. Rev. B* **37**, 1020 (1988).
- ⁵²J. Kakalios and W. B. Jackson, in *Advances in Amorphous Semiconductors: Amorphous Silicon and Related Materials* (Ref. 39), p. 207.
- ⁵³J. Kocka, M. Vanecek, and A. Triska, in *Advances in Amorphous Semiconductors: Amorphous Silicon and Related Materials* (Ref. 39), p. 297.
- ⁵⁴J. M. Marshall, R. A. Street, and M. J. Thompson, *Philos. Mag. B* **54**, 51 (1986).
- ⁵⁵K. Winer, I. Hirabayashi, and L. Ley, *Phys. Rev. Lett.* **60**, 2697 (1988); *Phys. Rev. B* **38**, 7680 (1988).
- ⁵⁶W. B. Jackson, S. M. Kelso, C. C. Tasi, J. W. Allen, and S. J. Oh, *Phys. Rev. B* **31**, 5187 (1985).
- ⁵⁷R. A. Street, D. K. Biegelsen, W. B. Jackson, N. M. Johnson, and M. Stutzmann, *Philos. Mag. B* **52**, 235 (1985).
- ⁵⁸H. Dersch, J. Stuke, and J. Beichler, *Phys. Status Solidi B* **105**, 265 (1981).
- ⁵⁹R. A. Street, M. Hack, and W. B. Jackson, *Phys. Rev. B* **37**, 4209 (1988).
- ⁶⁰T. Tiedje, J. M. Cebulka, D. L. Morel, and B. Abeles, *Phys. Rev. Lett.* **46**, 1425 (1981).
- ⁶¹D. Goldie and W. E. Spear, *Philos. Mag. Lett.* **57**, 135 (1988).
- ⁶²A. C. Hourd and W. E. Spear, *Philos. Mag. B* **51**, L13 (1985).
- ⁶³J. Kakalios and R. A. Street, *Phys. Rev. B* **34**, 6014 (1986).
- ⁶⁴J. Stuke, *J. Non-Cryst. Solids* **97&98**, 1 (1987).
- ⁶⁵M. Stutzmann, *Philos. Mag. B* **53**, L15 (1986).
- ⁶⁶W. B. Jackson, N. M. Amer, A. C. Boccara, and D. Fournier, *Appl. Opt.* **20**, 1333 (1981).
- ⁶⁷A. C. Boccara, D. Fournier, and J. Badoz, *Appl. Phys. Lett.* **36**, 130 (1980).
- ⁶⁸A. C. Boccara, D. Fournier, W. B. Jackson, and N. M. Amer, *Opt. Lett.* **5**, 377 (1980).
- ⁶⁹H. Matsumura, M. Maeda, and S. Furukawa, *J. Non-Cryst. Solids* **59&60**, 517 (1983).
- ⁷⁰R. A. Street, C. C. Tsai, J. Kakalios, and W. B. Jackson, *Philos. Mag. B* **56**, 305 (1987).
- ⁷¹A. Skumanich, N. M. Amer, and W. B. Jackson, *Phys. Rev. B* **31**, 2263 (1985).
- ⁷²K. Winer and L. Ley, in *Advances in Amorphous Semiconductors: Amorphous Silicon and Related Materials* (Ref. 39), p. 365.
- ⁷³Z. E. Smith and S. Wagner, in *Advances in Amorphous Semiconductors: Amorphous Silicon and Related Materials* (Ref. 39), p. 409.
- ⁷⁴Y. Bar-Yam, D. Adler, and J. D. Joannopoulos, *Phys. Rev. Lett.* **57**, 467 (1986).

- ⁷⁵L. Ley and K. Winer, in *Proceedings of the 19th International Conference on the Physics of Semiconductors*, edited by W. Zawadzki (PIOP, Warsaw, 1989) p. 1633.
- ⁷⁶I. Sakata, Y. Hayashi, M. Yamanaka and M. Satoh, *IEEE Electron Devices Lett.* **EDL-6**, 166 (1985).
- ⁷⁷W. B. Jackson and N. M. Amer, *Phys. Rev. B* **25**, 5559 (1982).
- ⁷⁸R. A. Street, D. K. Biegelsen, and J. C. Knights, *Phys. Rev. B* **24**, 969 (1981).
- ⁷⁹J. M. Marshall, R. A. Street, and M. J. Thompson, *Phys. Rev. B* **29**, 2331 (1984).